Submitted for publication in ApJL
Preprint typeset using LaTeX style emulateapj v. 12/16/11

THE PLACE OF THE LOCAL GROUP IN THE COSMIC WEB

XXXX[1], YYYY[2], ZZZZ[3]

Submitted for publication in ApJL

ABSTRACT

This

Subject headings: galaxies: Local Group — dark matter

1. INTRODUCTION

The configuration of galaxies in the Local Group (LG hereafter) is quite rare to find in the local Universe and in cosmological simulations. The LG is dominated by the two big spirals MW and M31, the next most-luminous galaxy is M33 which is $\sim$ 10 times less massive than M31, followed by several less luminous dwarf galaxies, up to a distance of $\sim$ 3Mpc. The velocity vector of M31, with a low tangential velocity is consistent to a head-on collision orbit toward the MW (Cox & Loeb 2008; van der Marel et al. 2012; Sohn et al. 2012).

Another feature of the Local group is the relatively low velocity dispersion of nearby galaxies up to $\sim$ 8 Mpc (Sandage & Tammann 1975; Aragon-Calvo et al. 2011, and references therein). Environment around the Local Group has density quite close to the average density of the universe (Klypin et al. 2003; Karachentsev 2005). In addition, the closest massive galaxy cluster, the Virgo Cluster, is $\approx$ 16.5 Mpc away (Mei et al. 2007).

All this combination of features make LG analogues very rare to find. Using numerical simulatons González et al. (2013a) found less than 2% MW-sized halos reside in a pair similar to MW-M31 and in a similar environment. Furthermore, if we select pairs constrained within 2σ error fron current observational measurements of the velocity components and distance to M31, there are only 88 systems in a cube of 250 h^{-1}Mpc side.

Forero-Romero et al. (2013) also study MW-M31 pairs in numerical simulations finding the typical quantities characterizing the orbital parameters of the LG are rare among typical pairs, but not enough to challenge the ΛCDM model. Another definition of LG analogues is made by Li & White (2008), but despite differences ocurr in the definitions and resulting fraction of LG analogues, all are in agreement with a low frequency of these pairs.

To understand better the properties of the LG and how this uncommon pair configuration fit in the cosmological context, an immediate question arise. What else can we say of the LG at larger scales?. In particular, which are the typical/prefered locations of these systems within the Cosmic Web?.

Looking the LG at larger scales we have it is located in a difuse and warped filament/wall conecting Virgo Cluster with Fornax Cluster, some nearby galaxies and groups members of this large structure are the Maffei group, NGC 6744, NGC 5128, $M101$, $M81$, $NGC1023$, Cen A group. At this scale, there is no evident alignment of the MW-M31 orbital plane with the local filament or the Virgo-Fornax direction.

However, if we look in a smaller volume below scales of $\sim$ 6 Mpc, there is a clear alignment of th the MW-M31 orbit with a local plane as shown by figure 3 in Courtois et al. (2013).

In this paper we will study the large scale environment of LG analogues using the Bolshoi simulation, in particular which kind of structures they reside and if there is any correlation or alignment with the cosmic web. Environment is defined by the cosmic web components identified by Forero-Romero et al. (2009), and we use the LG analogues computed by González et al. (2013a).

Paper is organized ...

2. SIMULATION AND WEB FINDING ALGORITHM

2.1. *The Bolshoi simulation*

We use the Bolshoi simulation of ΛCDM cosmology: $\Omega_{\rm m} = 1 - \Omega_\Lambda = 0.27$, $H_0 = 70\,{\rm km/s/Mpc}$, $\sigma_8 = 0.82$, $n_s = 0.95$ (Klypin et al. 2011), compatible with the constraints from the WMAP satellite (Hinshaw et al. 2013). The simulation followed evolution of dark matter in a $250h^{-1}$Mpc box with spatial resolution of $\approx 1h^{-1}$ kpc and mass resolution of $m_{\rm p} = 1.35 \times 10^8$ M$_\odot$. Halos are identified with the BDM algorithm (Klypin & Holtzman 1997). The BDM algorithm is a spherical overdensity halo finding algorithm and is designed to identify both host halos and subhalos.

2.2. *Cosmic web identification*

The web finding algorithm is based on the tidal tensor computed as the Hessian of the gravitational potential field

$$T_{ij} = \frac{\partial^2 \phi}{\partial r_i \partial r_j}, \quad (1)$$

where r_i, $i = 1, 2, 3$ refers to the three spatial comoving coordiates and ϕ is the gravitational potential renormalized to follow the following Poisson equation $\nabla\phi = \delta$ where δ is the matter overdensity.

This tensor is real and symmetric, which means that can be diagonalized. We note the eigenvalues $\lambda_1 \geq \lambda_2 \geq \lambda_3$ and their corresponding eigenvectors $\hat{e}_1$, $\hat{e}_2$ and $\hat{e}_3$. The web classification compares each one of the three eigenvalues to a threshold value $\lambda_{\rm th}$. If the three, two, one or zero eigenvalues are larger than this threshold the region es classified as peak, filament, sheet or void, respectively.

In Forero-Romero et al. (2009) we perform a detailed study for the topology of the cosmic web and its visual

[1] Uni A
[2] Uni B
[3] Uni C

counterpart as a function of the parameter $\lambda_{\rm th}$. We find that reasonable results in terms of the volume fraction occupied by voids, the visual inspection and the halo populations in each web type can be reached by values of $0.2 < \lambda_{\rm th} < 0.4$. In this paper we choose the value of $\lambda_{\rm th} = 0.3$. We have veryfied that the main trends reported in this paper are unsensitive to the choice of that parameter, as long as it is in the range already quoted.

The ellipticity and the prolatenes are quantities that measure the relative strength of the three eigenvalues. They are defined as follows

$$e = \frac{\lambda_3 - \lambda_1}{2(\lambda_1 + \lambda_2 + \lambda_3)}, \quad (2)$$

$$p = \frac{\lambda_1 + \lambda_3 - 2\lambda_2}{2(\lambda_1 + \lambda_2 + \lambda_3)}. \quad (3)$$

The algorithm to compute the potential is grid based. First we interpolate the density into a cubic grid and smooth it with a gaussian kernel. Then we obtain the gravitational potential and use finite differences to compute the Hessian at every point in the grid. Physically speaking, the cosmic web features are scale dependent and the grid size has to be chosen with respect to the physical scales of the problem at hand.

In our case we have used a grid size on and a gaussian smoothing with two times larger as the typical separation between the two halos in the Local Group. The objective is to have both halos in the pair a common environment. In this paper we use a grid spacing of $s = 1.024\ h^{-1}$Mpc , corresponding to a 256^3 grid in the Bolshoi volume. The scale for the gaussian smoothing uses the same value.

3. LOCAL GROUP ANALOGUES

To construct a sample of the MW-M31 pairs at $z \approx 0$, we use a series of simulation snapshots at $z < 0.1$ (i.e. in the last ≈ 1.3 Gyr before present) spaced by $\approx 150 - 250$ Myr. This is done because a particular configuration of MW and M31 is transient and would correspond to a relatively small number of systems at one snapshot. By using multiple snapshots we can increase the sample of systems in such configuration during a period of time in which secular cosmological evolution is small.

Pairs are selected allowing a wide range of masses, following an isolation critera, constraining by orbital measurements such as radial, tangential velocity and separation of the pair, and local environment constrains such as local velocity dispersion and local overdensity within a sphere of radius 5 Mpc. A full description of the selection criteria can be found in González et al. (2013a,b).

We define two samples according to the tolerance in the selection constraints: A sample named 2σ, correspondig to LG analogues constrained by two times the observational errors in the orbital values (radial velocity, tangential velocity, and separation), and a more relaxed sample named 3σ for LG analogues constrained by three times observational errors accordingly. The number of pairs in each sample is 46 and 120 respectively, notice we have less pairs than in González et al. (2013a) results, since we removed pairs which are too close at $z = 0$, i.e. their virial radii overlaps, also we removed a couple pairs who merged or change their mass more than 20% at present time since they were detected at $z < 0.1$.

Sample	Peak	Filament	Sheet	Void
	n (%)	n (%)	n (%)	n (%)
2σ	4 (8.5)	24 (51.0)	18 (38.2)	1 (2.1)
3σ	10 (8.1)	59 (48.3)	48 (39.3)	5 (4.0)
General	1307 (23.8)	1470 (26.8)	1769 (32.3)	927 (16.9)

TABLE 1
NUMBER OF PAIRS IN THE FOUR DIFFERENT KINDS OF ENVIRONMTNS. IN PARETHESIS THE SAME NUMBER AS A PERCENTAGE OF THE TOTAL POPULATION.

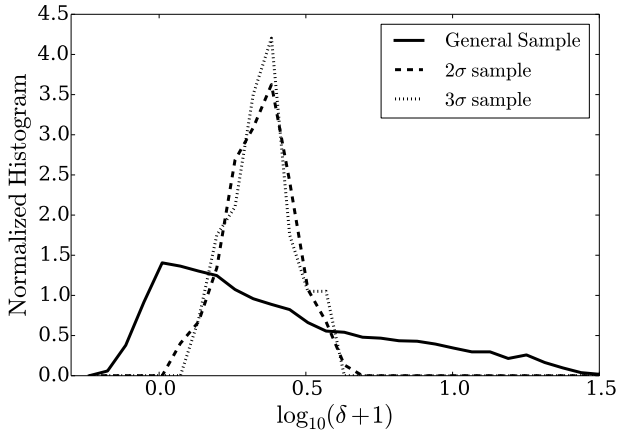

FIG. 1.— Overdensity distribution for the pairs in the three samples.

4. RESULTS

4.1. *Pairs in Filaments and Sheets*

The first result we explore is the kind of environment occupied by our LGs. We find that LGs in the restricted 2σ and 3σ samples prefer by large to be in filaments and sheets. Almost $\sim 50\%$ of the pairs in both cases can be found in filaments while $\sim 40\%$ can be found in sheets. This proportion is in stark contrast to the environments for the general pair sample. In that case only $\sim 27\%$ and $\sim 33\%$ can be found in filaments and sheets, repectively. There is a considerable fraction of pairs that are located in peaks ($\sim 25\%$) and voids ($\sim 15\%$). These results and the exact numbers are presented in Table 1.

4.2. *Overdensity, Ellipticity and Anisotropy*

The next result is related to the matter overdensity for the LG samples. Figure 1 shows that the range of overdensities for the general pair sample spans almost two orders of magnitude from underdense regions $\delta < 0$ to high density regions $\delta \sim 30$, with a distribution peaking around $\delta \sim 0$. In contrast the 2σ and 3σ samples are located within a narrower range of overdensities $0.0 < \delta < 4.0$ peaking at $\delta \sim 1.5$. These values are consistent with the fact that these samples are mostly found in filaments and sheets.

In Figure **??** we show the integrated distribution for the Fractional Anisotropy in the tree samples. The General Sample clusters towards values of $\mathrm{F}A \sim 1.0$, while the 2σ and 3σ prefer values around 0.6.

In Figure **??** we present a joint scatter plot for the overdensity and fractional anisotropy. For clarity we only include the general and 3σ samples. In this plane we

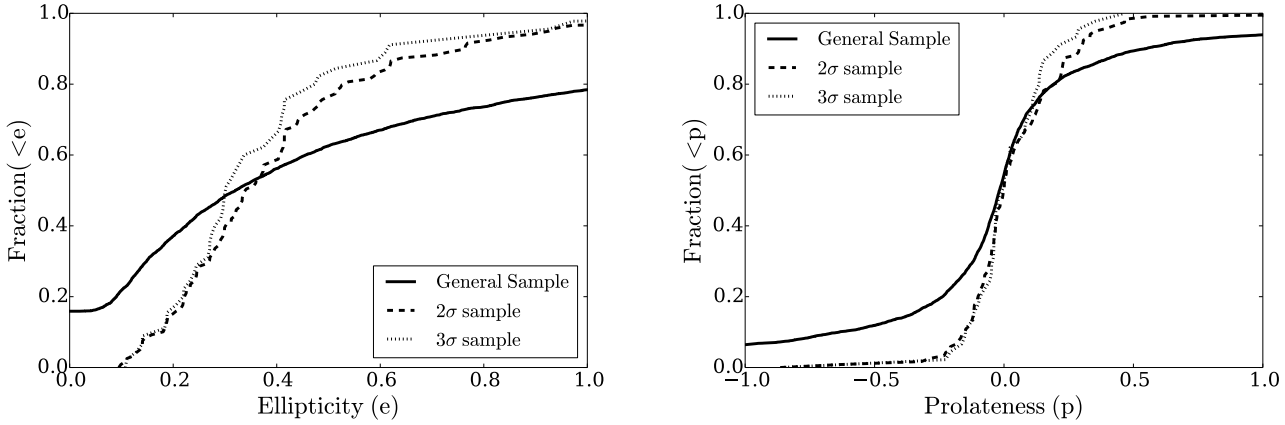

FIG. 2.— Cumulative distributions for the ellipticity and prolateness.

Sample	$\langle \hat{e}_1 \cdot \hat{n} \rangle$	$\langle \hat{e}_2 \cdot \hat{n} \rangle$	$\langle \hat{e}_3 \cdot \hat{n} \rangle$
2σ	0.56	0.53	0.33
3σ	0.51	0.51	0.46
General	0.54	0.52	0.40

TABLE 2
AVERAGE VALUES FOR THE COSINUS BETWEEN THE THREE EIGENVECTORS AND THE VECTOR NORMAL TO THE ORBITAL PLANE.

observe from the general sample that there are broad correlations between the overdensity and the fractional anisotropy.

4.3. *Alignment along the cosmic web*

5. DISCUSSION

6. CONCLUSIONS

ACKNOWLEDGEMENTS

REFERENCES

Aragon-Calvo, M. A., Silk, J., & Szalay, A. S. 2011, MNRAS, 415, L16
Courtois, H. M., Pomarède, D., Tully, R. B., Hoffman, Y., & Courtois, D. 2013, AJ, 146, 69
Cox, T. J., & Loeb, A. 2008, MNRAS, 386, 461
Forero-Romero, J. E., Hoffman, Y., Bustamante, S., Gottlöber, S., & Yepes, G. 2013, ApJ, 767, L5
Forero-Romero, J. E., Hoffman, Y., Gottlöber, S., Klypin, A., & Yepes, G. 2009, MNRAS, 396, 1815
González, R. E., Kravtsov, A. V., & Gnedin, N. Y. 2013a, ArXiv e-prints
—. 2013b, ApJ, 770, 96
Hinshaw, G., Larson, D., Komatsu, E., Spergel, D. N., Bennett, C. L., Dunkley, J., Nolta, M. R., Halpern, M., Hill, R. S., Odegard, N., Page, L., Smith, K. M., Weiland, J. L., Gold, B., Jarosik, N., Kogut, A., Limon, M., Meyer, S. S., Tucker, G. S., Wollack, E., & Wright, E. L. 2013, ApJS, 208, 19
Karachentsev, I. D. 2005, AJ, 129, 178
Klypin, A., Hoffman, Y., Kravtsov, A. V., & Gottlöber, S. 2003, ApJ, 596, 19
Klypin, A., & Holtzman, J. 1997, ArXiv Astrophysics e-prints
Klypin, A. A., Trujillo-Gomez, S., & Primack, J. 2011, ApJ, 740, 102
Li, Y.-S., & White, S. D. M. 2008, MNRAS, 384, 1459
Mei, S., Blakeslee, J. P., Côté, P., Tonry, J. L., West, M. J., Ferrarese, L., Jordán, A., Peng, E. W., Anthony, A., & Merritt, D. 2007, ApJ, 655, 144
Sandage, A., & Tammann, G. A. 1975, ApJ, 196, 313
Sohn, S. T., Anderson, J., & van der Marel, R. P. 2012, ApJ, 753, 7
van der Marel, R. P., Fardal, M., Besla, G., Beaton, R. L., Sohn, S. T., Anderson, J., Brown, T., & Guhathakurta, P. 2012, ApJ, 753, 8

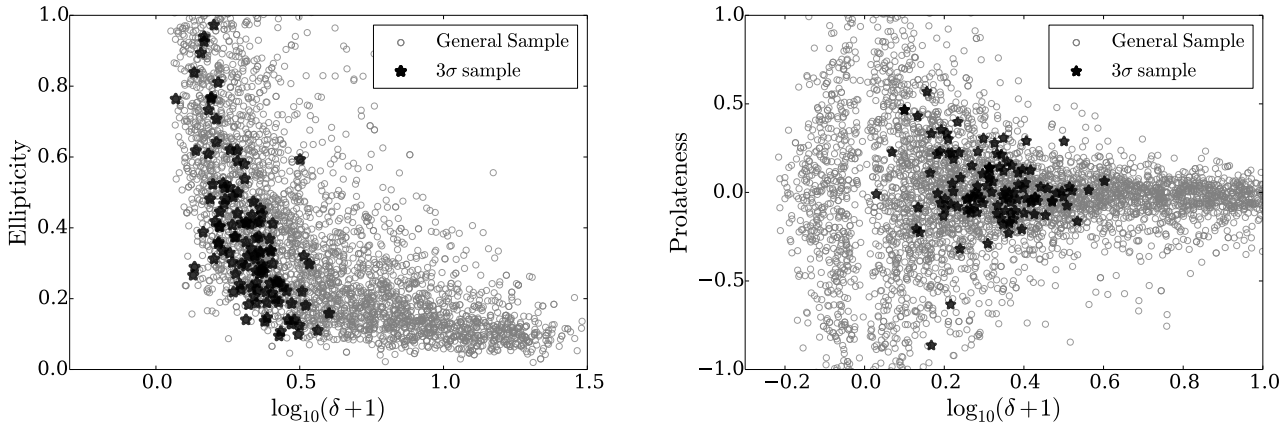

FIG. 3.— Ellipticity and prolateness versus the overdensity for the pairs in the general and 3σ samples.

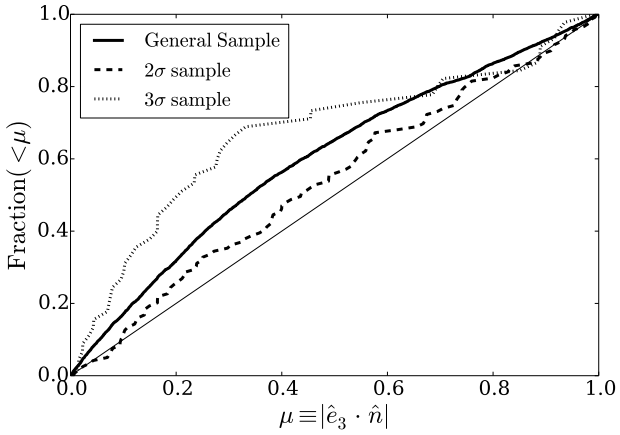

FIG. 4.— Cumulative distributions for the alignment between the normal vector $\hat{n}$ and the third eigenvector $\vec{e}_3$.